- 1.2. Starting with Eq. (1.2), derive Eq. (1.6), and use it to show that $r_d = 1.11r_e$.
- 1.3. Based on the values in Table 1.1 and below, calculate the Einstein frequency and the Debye frequency for copper, silver and gold and compare these values.

Element	$n (10^{22}/\text{cm}^3)$	Atomic Weight	$T_{\theta}(K)$
Cu	8.45	63.5	343
Ag	5.85	107.9	225
Au	5.9	197	165

- 1.4. Using the Lennard-Jones potential with $n = 8 \times 10^{22}$ atoms/cm³, $\epsilon_b = 0.6$ eV/atom and $r_e = (1/n)^{1/3}$:
 - (a) Calculate the maximum force F_{max} .
 - (b) Assume the solid is in the linear elastic region and calculate Young's modulus Y.
 - (c) What is the elastic energy E_{el} at F_{max} ?
- 1.5. (a) For the Lennard-Jones potential, discuss the influence of increasing the attractive interaction while keeping the repulsive interaction fixed. How will this effect the equilibrium separation r_e and the pair potential ϵ_h ?
 - (b) Repeat this process but decrease the repulsive interaction and do this while keeping the attractive interaction constant.
- 1.6. Suppose an atomic cluster of only 12 atoms forms. Assuming that the atoms can be described by the Lennard-Jones potential, would you expect the interatomic spacing and elastic modulus of the cluster to be greater or less than that of a corresponding bulk crystal? Explain.
- 1.7. Estimate the bond energies ϵ_b of copper, silver and gold from the heats of melting of the elements, assuming that there are 11 nearest neighbors in the liquid. How do your results compare with the values in Table 1.1?

REGULAR SOLUTION (QUASI-CHEMICAL) MODEL

Certain properties of binary solutions are used frequently in this book to explain phenomena such as segregation to interfaces and chemical gradients at interfaces. Thus, it is important that the reader be familiar with properties of binary solutions. This chapter summarizes some of the most important of these properties, including the regular solution model and the effect of temperature on solid solubility and also includes a brief review of some thermodynamics which lead up to the regular solution model. Our treatment is based on that of Porter and Easterling [12] and the reader may refer to this and other books on thermodynamics [2,13,14] for additional background.

2.1. THE GIBBS FREE ENERGY OF BINARY SOLUTIONS

In alloys, the Gibbs free energy is a function of composition, temperature and pressure. In this book, the pressure is usually assumed to be 1 atm and the reaction is carried out at constant temperature, so that these variables are fixed. In this case, the relative stability of a system is determined by its Gibbs free energy, which is defined as

$$G = H - TS, (2.1)$$

where H is the enthalpy, T is the absolute temperature and S is the entropy of the system. The quantity G is usually expressed in joules per mole. Enthalpy is a measure of the heat content of the system and is given by

$$H = E + PV. (2.2)$$

2.2. IDEAL SOLUTIONS

where E is the internal energy of the system, P is the pressure and V is the volume. The internal energy E arises from the total potential and kinetic energies of the atoms in a solid. Because the kinetic energy of the atoms is usually small compared to the interatomic potential energy, it is often neglected, as in the treatment of atomic bonding in the previous section. The heat that is absorbed or evolves during a reaction depends on the change in internal energy of the system. Most of the reactions of interest to this subject occur at a constant pressure of 1 atm and the PV term is usually very small in comparison with E when dealing with condensed phases (solids and liquids) so that $H \cong E$. We often use this approximation, and in fact have already used it in Section 1.2.1.

The Gibbs free energy of a binary solution of A and B atoms can be calculated from the free energies of pure A and pure B as follows. Assume that A and B have the same crystal structures in their pure states and that they can be mixed in any proportion to make a homogeneous solid solution with the same crystal structure. Mixing together X_A moles of A and X_B moles of B to form 1 mole of solid solution gives

$$X_A + X_B = 1,$$
 (2.3)

where X_A and X_B are the mole fractions of A and B in the alloy. To calculate the free energy of the alloy, the mixing can be envisioned to occur in two steps: (a) bring together X_A moles of pure A and X_B moles of pure B and (b) allow the A and B atoms to mix together to make a homogeneous solid solution. After step (a), the free energy of the system is given by

$$G_1 = X_A G_A + X_B G_B, \tag{2.4}$$

where G_A and G_B are the molar free energies of pure A and pure B at 1 atm and the temperature of interest. The quantity G_1 can be conveniently represented on a molar free energy diagram, where the molar free energy is plotted as a function of mole fraction X_B , as shown in Figure 2.1. In this case, G_1 lies on a straight line between G_A and G_B for all alloy compositions.

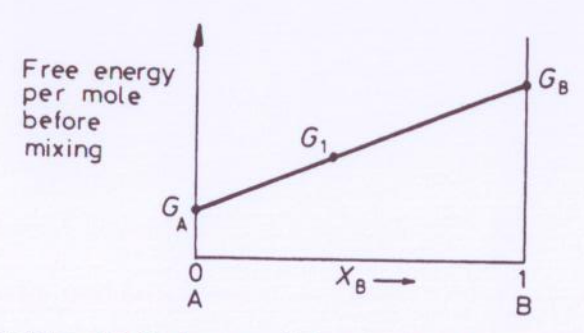


Figure 2.1. Variation of G_1 (the free energy before mixing) with alloy composition X_B (or X_A). From [12].

When the A and B atoms are allowed to mix in step (b) above, the free energy of the solid solution changes so that the resulting Gibbs free energy after mixing G_2 is given as

$$G_2 = G_1 + \Delta G_{\text{mix}}, \tag{2.5}$$

where ΔG_{mix} is the change in Gibbs free energy caused by mixing. Rearranging Eq. (2.5) so that

$$\Delta G_{\rm mix} = G_2 - G_1$$

and letting

$$\Delta H_{\text{mix}} = H_2 - H_1$$
 and $\Delta S_{\text{mix}} = S_2 - S_1$

then gives (from Eq. 2.1),

$$\Delta G_{\text{mix}} = \Delta H_{\text{mix}} - T \Delta S_{\text{mix}}, \qquad (2.6)$$

where ΔH_{mix} is the heat absorbed or evolved during step (b) (i.e., it is the heat of solution). Ignoring the volume change during the process (PV), it represents only the difference in internal energy (E) before and after mixing. ΔS_{mix} is the difference in entropy between the mixed and unmixed states.

2.2. IDEAL SOLUTIONS

The simplest type of mixing occurs for a so-called ideal solution where $\Delta H_{\rm mix} = 0$ and the free energy change on mixing is due only to the change in entropy

$$\Delta G_{\text{mix}} = -T\Delta S_{\text{mix}}.$$
 (2.7)

There are two contributions to the entropy, a thermal contribution and a configurational contribution. If there is no volume or heat change during mixing then the only contribution to $\Delta S_{\rm mix}$ is the change in configurational entropy. The configurational entropy is quantitatively related to the randomness of the solid solution by the Boltzmann equation

$$S = k_{\rm B} \ln \xi, \tag{2.8}$$

where k_B is Boltzmann's constant and ξ is the number of distinguishable ways of arranging the atoms in the solid solution. Assuming that A and B atoms mix to form a substitutional solid solution where all configurations of A and B atoms are equally probable gives an expression for ΔS_{mix} (see [12–14])

$$\Delta S_{\text{mix}} = -R(X_A \ln X_A + X_B \ln X_B). \tag{2.9}$$

Note that since X_A and X_B are less than unity, ΔS_{mix} is positive and there is an increase in entropy on mixing as expected physically. The free energy on mixing is then obtained from Eq. (2.7) as

$$\Delta G_{\text{mix}} = RT(X_A \ln X_A + X_B \ln X_B). \tag{2.10}$$

The actual free energy of the solution depends on G_A and G_B and combining Eqs. (2.4), (2.5) and (2.10) yields

$$G = G_2 = X_A G_A + X_B G_B + RT(X_A \ln X_A + X_B \ln X_B), \tag{2.11}$$

which is illustrated graphically as a function of temperature and composition in Figure 2.2.

2.3. CHEMICAL POTENTIAL

In alloys, we are often interested in knowing how the free energy of a particular phase changes when atoms are added or removed. If a small quantity of element A, say dn_A moles, is added to a large amount of phase at constant temperature and pressure, the size of the system increases by dn_A and there is an increase dG' in the total free energy of the system. (The symbol G' has been used for the Gibbs free energy to indicate that it refers to the whole system since the usual symbol G, which indi-

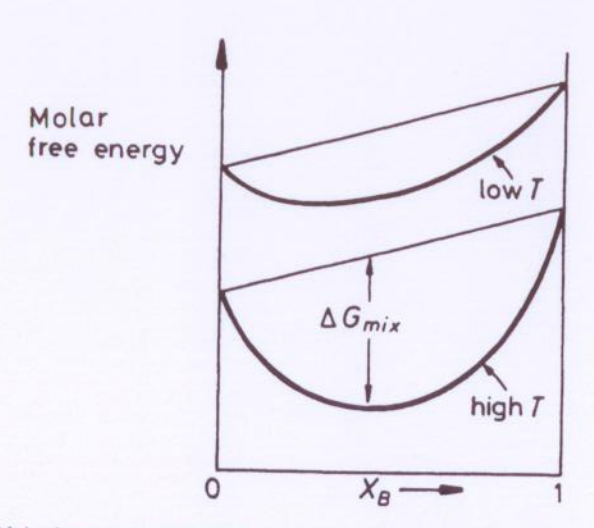


Figure 2.2. Molar free energy of mixing for an ideal solid solution where $\Delta H_{\text{mix}} = 0$. From [12].

cates the molar free energy is independent of the size of the system.) If dn_A is small enough, dG' is proportional to the amount of A added, and we can write

$$dG' = \mu_A dn_A \quad \text{(constant } T, P, n_B), \tag{2.12}$$

where the proportionality constant μ_A is called the partial molar free energy of A, or alternatively, the chemical potential of A in the phase. Because μ_A depends on the composition of the phase, dn_A must be infinitesimally small so that the composition of the phase is not altered significantly. Rearranging Eq. (2.12) then gives a definition for the chemical potential as

$$\mu_A = \left(\frac{\partial G'}{\partial n_A}\right)_{T,P,n_B}.\tag{2.13}$$

Equations similar to Eqs. (2.12) and (2.13) can be written for the other components in the solution. When this is done for a binary solution at constant temperature and pressure, we obtain

$$dG' = \mu_A dn_A + \mu_B dn_B. \tag{2.14}$$

If A and B atoms are added to a solution in the same proportion as the original composition of the solution (i.e., such that the ratio $dn_A/dn_B = X_A/X_B$), then the free energy of the solution increases by the molar free energy G. Thus, from Eq. (2.14),

$$G = \mu_A X_A + \mu_B X_B. \tag{2.15}$$

When G is known as a function of X_A and X_B as in Figure 2.2 for example, μ_A and μ_B can be obtained by extrapolating the tangent to the G curve to the sides of the molar free energy diagram as shown in Figure 2.3. It then becomes evident that μ_A and μ_B vary systematically with the composition of the phase X_B .

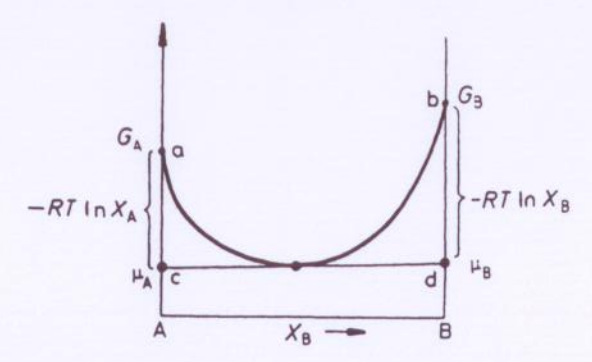


Figure 2.3. Illustration of the relationship between the free energy curve and the chemical potentials for an ideal solution. From [12].

Comparison of Eqs. (2.11) and (2.15) gives μ_A and μ_B for an ideal solution as

$$\mu_A = G_A + RT \ln X_A$$
 and $\mu_B = G_B + RT \ln X_B$, (2.16)

which is a simple way of representing Eq. (2.11). These relationships are also shown on the free-energy-composition diagram in Figure 2.3, where the distances ac and bd are $-RT \ln X_A$ and $-RT \ln X_B$, respectively.

2.4. REGULAR SOLUTIONS

Now we are ready to consider the regular solution or quasi-chemical model for a binary alloy solution, the result we really want to utilize in this book. So far, it has been assumed that $\Delta H_{\rm mix}=0$. This occurs rarely and mixing is usually endothermic (heat absorbed) or exothermic (heat evolved). However, we can readily extend the simple model developed for an ideal solution to include $\Delta H_{\rm mix}$ using the so-called quasi-chemical (or Bragg-Williams) approach, which is basically a nearest-neighbor bond-counting approach to alloying.

In the quasi-chemical model, it is assumed that the heat of mixing ΔH_{mix} is only due to the bond energies of adjacent atoms. For this assumption to be valid, it is necessary that the volumes of pure A and B are equal and do not change during mixing so that the interatomic distances and bond energies are independent of composition.

The structure of a simple, binary solid solution is shown in Figure 2.4. Three types of bonds are present in the structure:

- 1. A-A bonds, each with an energy ϵ_{AA}
- 2. B-B bonds, each with an energy ϵ_{BB}
- 3. A-B bonds, each with an energy ϵ_{AB} .

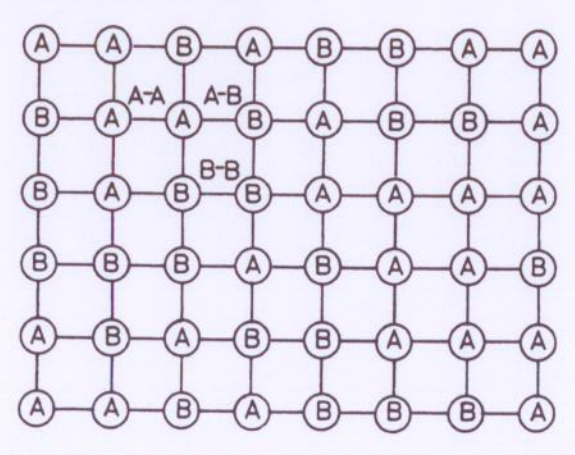


Figure 2.4. Different types of interatomic bonds in an A-B solid solution. From [12].

By considering zero energy as the state where the atoms are separated at infinity, ϵ_{AA} , ϵ_{BB} and ϵ_{AB} are negative quantities, which become increasingly more negative as the bonds become stronger. (Note that ϵ_{AA} and ϵ_{BB} can be estimated from Eq. 1.4). The internal energy of the solution E depends on the number of bonds of each type n_{AA} , n_{BB} and n_{AB} , such that

$$E = n_{AA} \epsilon_{AA} + n_{BB} \epsilon_{BB} + n_{AB} \epsilon_{AB}. \tag{2.17}$$

By considering the relationships among n_{AA} , n_{BB} and n_{AB} in the solution it can be shown [13] that the change in internal energy of the solution is given by

$$\Delta H_{\text{mix}} = n_{AB} \epsilon, \tag{2.18}$$

where

$$\epsilon = \epsilon_{AB} - \frac{1}{2}(\epsilon_{AA} + \epsilon_{BB}). \tag{2.19}$$

In other words, ϵ is the difference between the A-B bond energy and the average of the A-A and B-B bond energies. Note that the bond energies must be specified as negative quantities in Eq. (2.19) in order to be consistent with Figure 1.1a.

If $\epsilon = 0$, then $\Delta H_{\rm mix} = 0$, and the solution is ideal. In this case, the atoms are completely randomly arranged and the entropy of mixing is given by Eq. (2.9). If $\epsilon < 0$, the atoms in the solution prefer to be surrounded by atoms of the opposite type. This increases n_{AB} and the alloy tends to form an ordered solid solution. In contrast, if $\epsilon > 0$, the atoms prefer to be surrounded by atoms of their own kind. In this case, n_{AB} is less than in a random solid solution and the alloy tends toward phase separation or clustering (unmixing). Since the total number of atom pairs in a crystal is $\frac{1}{2} 2N_A$, the number of A-B pairs is equal to the total number of pairs multiplied by the probability that a pair is of the A-B type, or

$$n_{AB} = \frac{1}{2} z N_A (2X_A X_B) = z N_A X_A X_B.$$
 (2.20)

We therefore find that the heat of mixing is given as

$$\Delta H_{\text{mix}} = \Omega X_A X_B, \tag{2.21}$$

where the interaction parameter

$$\Omega = zN_{\mathbf{A}}\epsilon. \tag{2.22}$$

Real solutions that closely obey Eq. (2.21) are known as regular solutions. Since Ω is independent of composition, $\Delta H_{\rm mix}$ is a parabolic function of composition as shown in Figure 2.5. The sign of Ω indicates the same trend toward ordering or clustering as that of ϵ above. Note that the tangents at $X_B=0$ and 1 are related to the value of Ω as shown and that Ω is positive in this figure.

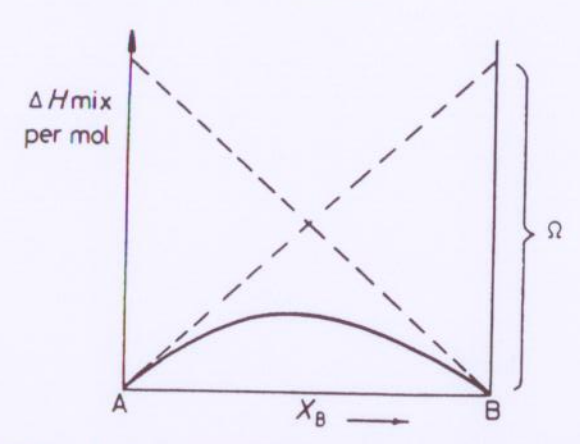


Figure 2.5. Variation of $\Delta H_{\rm mix}$ with composition for a regular solution. Note that Ω is given as $\partial \Delta H_{\rm mix}/\partial X_B$ at the limits of composition and that $\Omega = 4\Delta H_{\rm mix}$ at $X_B = 0.5$ From [12].

The free energy change on mixing for a regular solution is given by combining Eqs. (2.5), (2.9) and (2.21) as

$$\Delta G_{\text{mix}} = \Omega X_A X_B + RT(X_A \ln X_A + X_B \ln X_B), \tag{2.23}$$

which is shown in Figure 2.6 for different values of Ω and temperature. For exothermic solutions, $\Delta H_{\rm mix}$ (or Ω) < 0 and mixing results in a free energy decrease at all temperatures as in Figures 2.6a and b. This type of behavior is exhibited by the f.c.c. nickel–platinum system, for example [15]. When $\Delta H_{\rm mix} > 0$, at high temperatures $T\Delta S_{\rm mix}$ is greater than $\Delta H_{\rm mix}$ for all compositions and the free energy curve has a positive curvature at all points, as in Figure 2.6c. At low temperatures, $T\Delta S_{\rm mix}$ is smaller and $\Delta G_{\rm mix}$ develops a negative curvature in the middle, as in Figure 2.6d. This type of behavior is displayed by the f.c.c. gold–nickel system, for example [16].

It is important to note that both ordering of an alloy (increasing n_{AB}) and clustering (decreasing n_{AB}) lead to a decrease in the mixing entropy $\Delta S_{\rm mix}$ compared to that of a random solid solution, because the number of ways that the atoms can be arranged on a lattice decreases. In either case, an optimum degree of ordering or clustering will result, reflecting a balance between $\Delta H_{\rm mix}$ and $T\Delta S_{\rm mix}$ in order to minimize $\Delta G_{\rm mix}$. This factor is not taken into account in the quasi-chemical model. In addition, it is important to note that because the $\Delta S_{\rm mix}$ term in Eq. (2.9) and (2.23) is multiplied by T, the $T\Delta S$ term is more important at higher temperatures. As a result, the degree of ordering or clustering in a system decreases as the temperature increases. This is a very important point, because the same basic principle applies to other phenomena, such as segregation to interfaces or the sharpness of certain interfaces that tend to decrease with increasing temperature (see, for example, Sections 13.2.8 and 14.2).

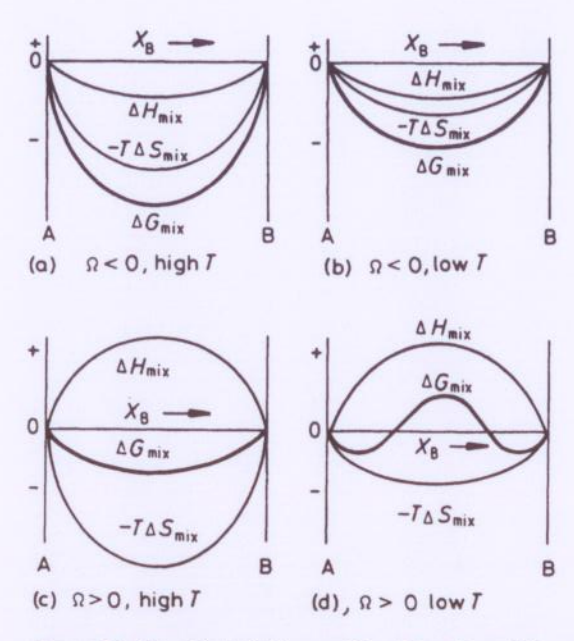


Figure 2.6. The effect of ΔH_{mix} and T on ΔG_{mix} . From [12].

The size difference between atoms is neglected in the quasi-chemical model and this has the effect of underestimating the change in internal energy on mixing, because the elastic strain fields that introduce a strain energy term into $\Delta H_{\rm mix}$ are not taken into account. When the size difference is large, this effect can dominate over the chemical term. Nevertheless, the quasi-chemical model is still appealing because of its conceptual and mathematical simplicity.

The actual free energy of an alloy depends on the values of G_A , G_B , and ΔG_{mix} and is obtained by combining Eqs. (2.4), (2.5) and (2.23) as

$$G = X_A G_A + X_B G_B + \Omega X_A X_B + RT(X_A \ln X_A + X_B \ln X_B). \tag{2.24}$$

Comparing Eqs. (2.15) and (2.24) and using the relationship $X_A X_B = X_A^2 X_B + X_B^2 X_A$ shows that for a regular solution

$$\mu_A = G_A + \Omega(1 - X_A)^2 + RT \ln X_A = G_A + RT \ln a_A$$

$$\mu_B = G_B + \Omega(1 - X_B)^2 + RT \ln X_B = G_B + RT \ln a_B, \qquad (2.25)$$

where a_A and a_B are defined as the activities of A and B, which are illustrated graphically in Figure 2.7. Rearrangement of Eqs. (2.25) yields the activity coefficients, γ_A and γ_B which account for the deviation of the regular solution from ideal behavior (Raoult's law) through the interaction parameter Ω . This topic is not elaborated here, but it is discussed further in thermodynamics texts [2,13,14].

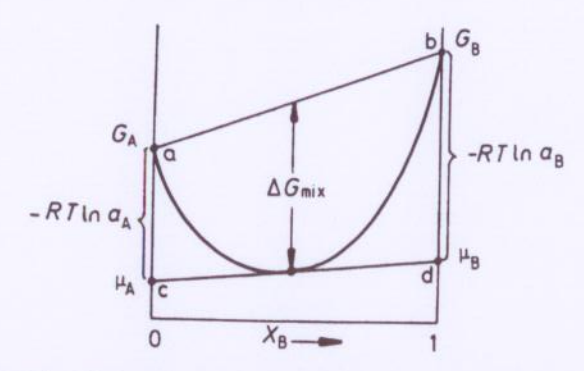


Figure 2.7. Relationship between the molar free energy and activity (compare with Fig. 2.3). From [12].

2.5. SYSTEMS WITH A MISCIBILITY GAP

Figure 2.8 shows the free energy curves and the resulting temperature-composition phase diagram for a system in which the liquid phase is approximately ideal but for the solid phase $\Delta H_{\text{mix}} > 0$ (i.e., the A and B atoms repel one another). At high temperatures such as T_1 in Figure 2.8d, the free energy curve for the liquid G^L lies below that of the solid G^S for all compositions (Fig. 2.8a) and the liquid phase is stable. At lower temperatures, such as T_2 in Figure 2.8d, G^S dips below G^L (Fig. 2.8b) and the alloy contains several different solid and liquid phases depending on the composition. From $X_B = 0$ to point a in Figure 2.8b the stable phase is solid α with the overall alloy composition. From points a to b, the common tangent construction indicates that at equilibrium the alloy consists of a two-phase mixture containing solid α and liquid with the compositions given by points a and b, respectively, on the temperature-composition diagram. Between points b and c, the liquid phase with the overall alloy composition is stable. The reverse trend in phases occurs with increasing composition X_B across the remainder of the diagram. At still lower temperatures such as T_3 , the free energy curve for the solid assumes a negative curvature in the middle as in Figure 2.8c, and the solid solution is most stable as a mixture of two phases α' and α'' with compositions given by the common tangent at eand f. At somewhat higher temperatures when $-T\Delta S_{mix}$ becomes larger, e and f approach each other and eventually disappear (at point g) as shown in the phase diagram in Figure 2.8d. The $\alpha' + \alpha''$ region is known as a miscibility gap.

The effect of a positive ΔH_{mix} in the solid is already apparent at higher temperatures where it gives rise to a minimum melting point mixture. Physically, it can be argued that the reason why the alloy melts below the melting points of the pure components at all temperatures is because the atoms repel each other, making it easier to break the bonds and disrupt the solid into a liquid.

The critical temperature $T_{\rm c}$ associated with the miscibility gap of the phase diagram in Figure 2.8d is largely determined by the magnitude of the heat of mixing. For purposes of illustration, we consider the miscibility gap of a regular solution.

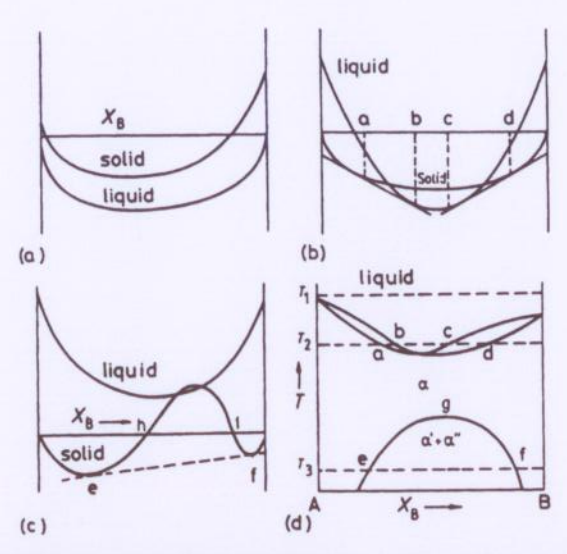


Figure 2.8. Derivation of a phase diagram where $\Delta H_{\text{mix}}^{\text{S}} > \Delta H_{\text{mix}}^{\text{L}} = 0$. Free energy versus composition curves for (a) T_1 , (b) T_2 and (c) T_3 . The resulting phase diagram as a function of temperature and composition is shown in (d). From [12].

We want to calculate the maximum critical temperature T_c where decomposition occurs and the composition X_B^c at this temperature (point g in Figure 2.8d). Above temperature T_c the curve of ΔG_{mix} versus X_B is everywhere concave downward. Below this temperature, two minima occur and there are two inflection points (labeled h and i in Figure 2.8c), where

$$\frac{\partial^2 \Delta G_{\text{mix}}}{\partial X_B^2} = 0. {(2.26)}$$

As the temperature is raised toward $T_{\rm c}$, the minima move closer together in composition and so do the inflection points. At $T_{\rm c}$, both minima and the inflection points coincide at the same temperature. Thus $T_{\rm c}$ is the temperature where both $\partial \Delta G_{\rm mix}/\partial X_B$ and $\partial^2 \Delta G_{\rm mix}/\partial X_B^2$ equal zero at the critical composition X_B^c . Performing these operations, we find

$$T_{\rm c} = 2X_B^{\rm c}(1 - X_B^{\rm c})\Omega/R.$$
 (2.27)

From Eq. (2.27) we see that Ω must be positive for T_c to be positive. Further, X_B^c is such that T_c is the maximum decomposition temperature associated with the miscibility gap. The value of X_B^c that makes T_c a maximum in Eq. (2.27) is $X_B^c = 0.5$, and thus

$$T_{\rm c} = \Omega/2R. \tag{2.28}$$

Clearly, T_c increases as ϵ_{AB} becomes more negative, i.e., as the energy of the A-B

pair increases in relation to the average of the A-A and B-B pairs. According to the quasi-chemical theory, a positive value of Ω indicates a repulsive interaction between unlike atoms. Thus, from Eq. (2.28), the larger this repulsive interaction, the higher the temperature will be where decomposition begins. If $\Delta H_{\rm mix} >> 0$, the miscibility gap in Figure 2.8d can extend into the liquid phase. In this case, a simple eutectic phase diagram results, as illustrated for different temperatures in Figure 2.9. A similar phase diagram can also result when A and B have different crystal structures, although we do not develop this case here. We return to discuss using the solvus lines in Figure 2.8d and Figure 2.9 to estimate $\Delta H_{\rm mix}$ in Section 2.8.

2.6. ORDERED ALLOYS

The opposite type of behavior occurs when $\Delta H_{\rm mix}$ < 0. In these systems, melting is more difficult and a maximum melting point mixture can appear. This type of alloy also has a tendency to order at low temperatures, as shown in Figure 2.10a. If the attraction between unlike atoms is very strong, the ordered phase may extend as far as the liquid, as illustrated in Figure 2.10b. Various types of order–disorder reactions can occur in solids. We examine the properties of antiphase boundaries (an interface between two ordered domains) later in this book, and so we examine some further properties of ordered alloys here [13].

Consider as an example an alloy containing 50 at.% A and 50 at.% B atoms that

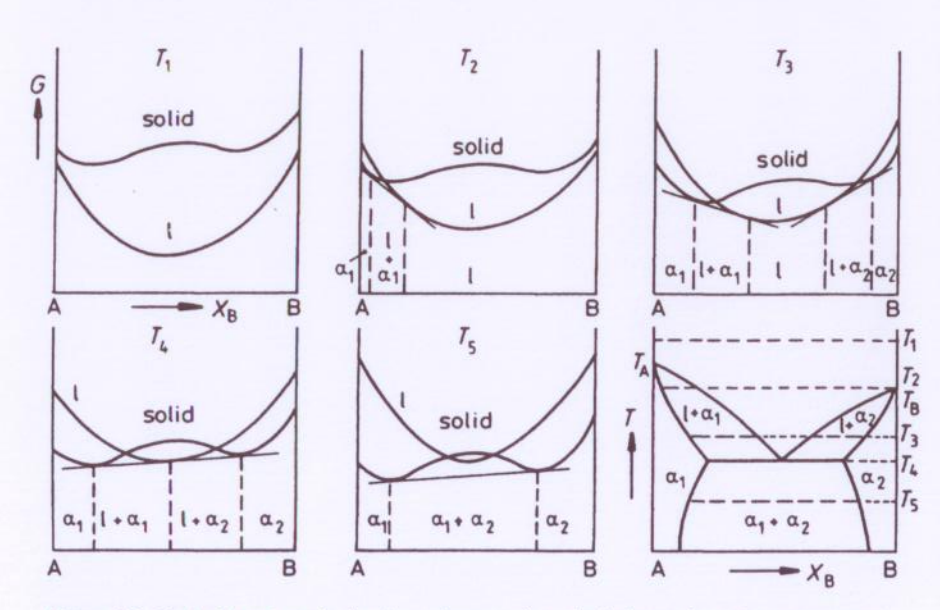


Figure 2.9. Derivation of a eutectic phase diagram where both phases have the same crystal structure. From [12].

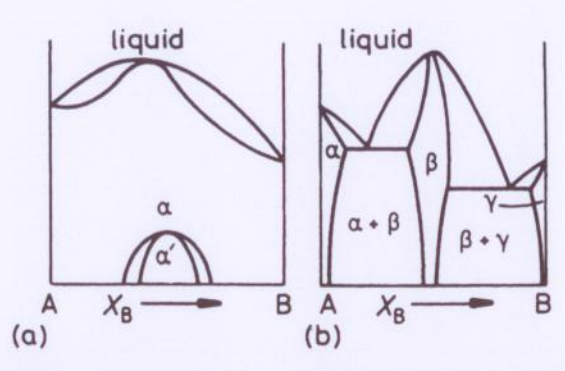


Figure 2.10. (a) Phase diagram when $\Delta H_{\text{mix}} < 0$. (b) Same as in (a) but with ΔH_{mix} even more negative. From [12].

tends to form an ordered phase. That is, the A atoms tend to order on one type of site α and the B atoms tend to order on another type of site β , as shown in Figure 2.11 for a b.c.c. structure. We denote the fraction of α sites occupied by the right (r) atoms (A atoms) as n_r^{α} and the fraction of β sites occupied by the right atoms (B atoms) as n_r^{β} . The fraction of α sites occupied by wrong (w) atoms (B atoms) is given as

$$n_w^{\alpha} = 1 - n_r^{\alpha}$$

and the fraction of β sites occupied by wrong atoms (A atoms) is

$$n_{\rm w}^{\beta}=1-n_{\rm r}^{\beta}.$$

For complete order, $n_r^{\alpha} = n_r^{\beta} = 1$ and for complete randomness, the probability that

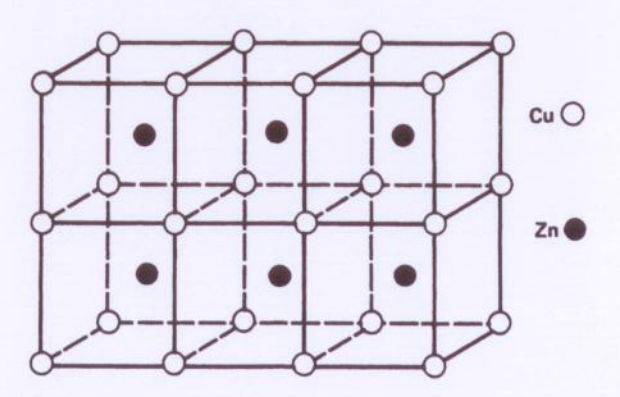


Figure 2.11. Long-range order on a b.c.c. lattice illustrated by the β -brass (copper-zinc) structure. From [2].

an α site is occupied by an A atom is X_A . Hence, the fraction of α sites occupied by A atoms for complete disorder is X_A . It is convenient to define a long-range order parameter $\mathfrak L$ in terms of order on the α sites as

$$\mathfrak{L} \equiv \frac{n_{\rm r}^{\alpha} - X_A}{1 - X_A} \tag{2.29a}$$

or, considering disorder on the B sites

$$\mathfrak{L} \equiv \frac{n_{\rm r}^{\beta} - X_B}{1 - X_B}.\tag{2.29b}$$

From Eqs. (2.29), we see that $\mathfrak{L}=0$ for complete disorder and $\mathfrak{L}=1$ for complete order. For a state of order given by $0 \le \mathfrak{L} \le 1$, the fraction of A atoms on sites α is n_r^{α} .

By considering the number of A-A pairs, B-B pairs and A-B pairs for an ordered alloy with long-range order parameter \mathfrak{L} , it is possible to show [13] that at any temperature different from T_c ,

$$\ln\frac{1+\mathfrak{L}}{1-\mathfrak{L}} = 2\mathfrak{L}\frac{T_{c}}{T}.$$
(2.30)

The formal derivation of Eq. (2.30) is known as the Bragg-Williams [17] or zeroth-order approximation. At low temperatures, $\mathfrak L$ is close to 1 and, as T increases toward $T_{\rm c}$, $\mathfrak L$ decreases very rapidly. This behavior is typical of a cooperative phenomenon. When order is perfect, it is difficult energetically to create disorder. However, as disorder proceeds, the process becomes progressively easier energetically until the case of complete disorder, where the energy becomes zero for the exchange process. The disordering energy thus depends on $\mathfrak L$.

A comparison between calculated (Eq. 2.30) and measured values of $\mathfrak L$ as a function of T is shown in Figure 2.12 for a 50 at.% copper–50 at.% zinc alloy. The long-range order parameter changes over a range of temperatures as indicated by Eq. (2.30). As a consequence, the transformation is not first order in nature and displays a discontinuity in the heat capacity as expected for a second-order transition.

It is possible to show that order-disorder transformations do not have to occur at precise chemical compositions but may occur over a composition interval. The further from the ideal proportion of A and B the actual composition is, the lower is the maximum value of $\mathfrak L$ and T_c , because $\mathfrak L$ cannot have the value of unity and some B atoms must reside on A sites and vice versa.

Order-disorder transformations are found in many different crystal systems. For example, there are transformations in the f.c.c. copper-gold system for alloy compositions of approximately 25, 50 and 75 at.% gold. These transformations appear to be first-order in nature and exhibit $\mathfrak{L}-T$ curves like that shown in Figure 2.13. The Bragg-Williams theory is not able to adequately explain these transformations, and one must resort to other theoretical treatments [2,13,14].

To illustrate the richness of the regular solution model, this section closes by showing the pattern of phase diagrams that can be generated from two phases α

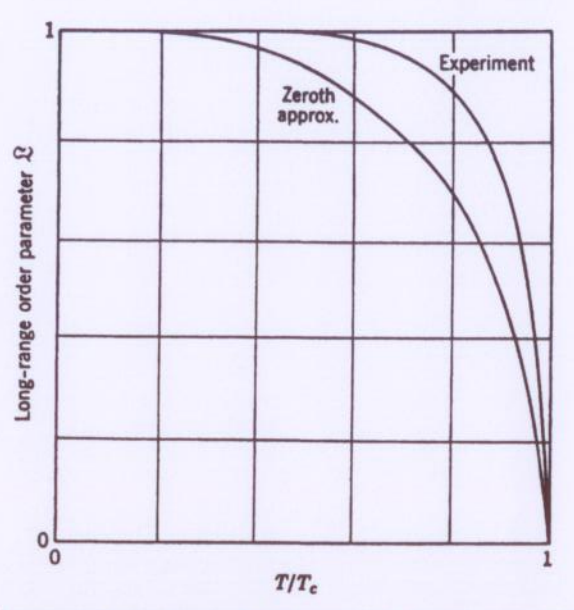


Figure 2.12. Long-range order parameter as a function of temperature for 50 at.% Cu–50 at.% Zn alloy. From [13] reprinted by permission of John Wiley & Sons, Inc.

(solid) and L using this simple model. All the diagrams in Figure 2.14 have the same melting points and entropies of fusion for the pure components. The pattern that develops is entirely due to variations in the interaction parameters for the solid and liquid, Ω^S and Ω^L , respectively. The top row of diagrams has a fixed positive value of Ω^S and each diagram thus has a miscibility gap in the solid solution with a critical temperature T_c . The diagrams in the bottom row are calculated with small values of Ω^S . The values of Ω^L were chosen so that the phase diagrams display an $(\alpha + L)$

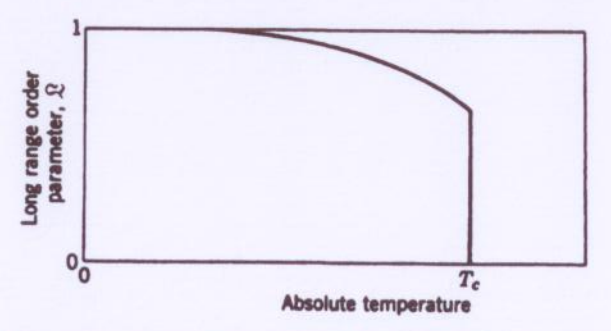


Figure 2.13. Long-range order parameter $\mathfrak L$ for an A_3B alloy. From [13] reprinted by permission of John Wiley & Sons, Inc.

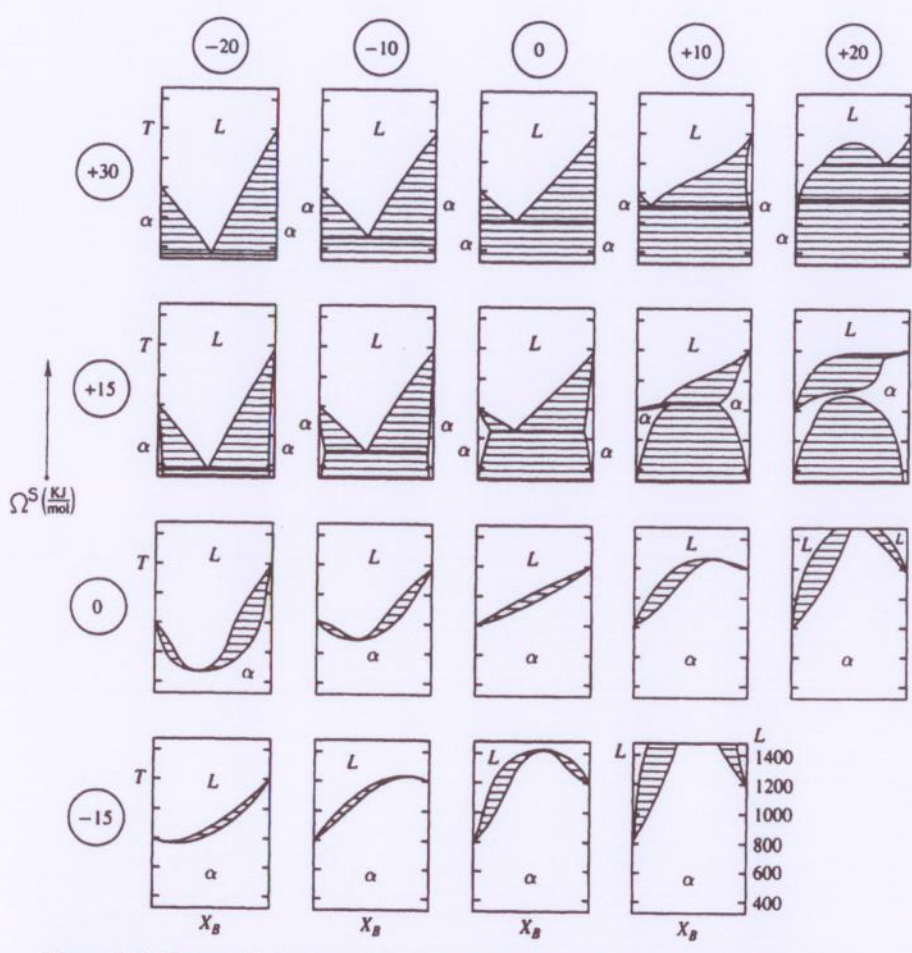


Figure 2.14. Pattern of phase diagrams that can be generated from only two phases α and L with the simple regular solution model. From [14], reprinted with permission of the McGraw-Hill Companies.

field with a minimum, monotectic and maximum from left to center to right, respectively.

2.7. EFFECT OF TEMPERATURE ON SOLID SOLUBILITY

It is possible to obtain several thermodynamic quantities, in particular Ω for a solid solution, from the solvus line in a phase diagram assuming a regular solution model; this is illustrated here because it is useful in determining ϵ_{AB} from Eq. (2.22). We consider the simplest case illustrated by the phase diagram in Figure

2.15, where component B is considered to be soluble to the extent of X_B^{sat} in α at a temperature T_1 , but A has an infinitesimal solubility in B. The treatment can be extended to include the situation where both α and β phases display some solubility.

Using statistical thermodynamics, it can be shown [13,14] that at equilibrium, the mole fraction of B in α , $X_B^{\rm sat}$, is given as

$$\ln X_B^{\text{sat}} = \frac{\Delta S_B}{k_B} - \frac{\Delta H_B}{k_B T},\tag{2.31}$$

where ΔH_B corresponds to the enthalpy expended in transfering pure B to the dilute solution. This is the relative partial molar enthalpy and as for most solid state reactions, ΔH_B is virtually independent of temperature. For a dilute solution in which the solute follows Henry's law (as assumed in the derivation of Eq. 2.31), ΔH_B is also independent of composition. The term ΔS_B represents the excess entropy of a solute in solution in α relative to the value of the pure solute and this includes the vibrational and configurational components of the entropy.

Experimentally, when $\ln X_B^{\rm sat}$ is plotted versus 1/T from the solvus line in the phase diagram, a straight line is obtained. From Eq. (2.31), it is evident that the slope of this line is ΔH_B and that ΔS_B can be obtained by extrapolating $X_B^{\rm sat}$ to 1/T=0 to find the intercept $\Delta S_B/k_B$. Generally, ΔH_B is positive for solid solutions, so $X_B^{\rm sat}$ increases with temperature. Figure 2.16 shows solubility data for various solutes in aluminum plotted this way. Most of these systems actually involve an equilibrium between a solid solution and an intermediate phase, or a phase with a crystal structure different from the α phase, rather than pure B with the same crystal structure. It is important to note that, in these cases, the heat of solution also includes a change in the standard state involved in converting 1 mole of B with the B structure into the B structure. If the difference in enthalpy between the B and B form of B is B in joules per mole), then

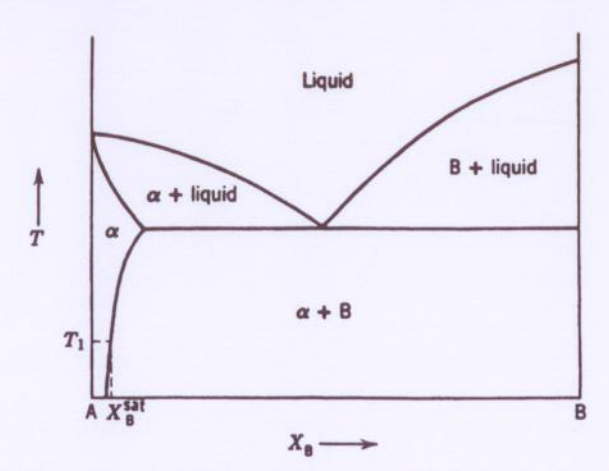


Figure 2.15. Phase diagram for the case where *B* is soluble in *A* but *A* is insoluble in *B*. From [13] reprinted by permission of John Wiley & Sons, Inc.

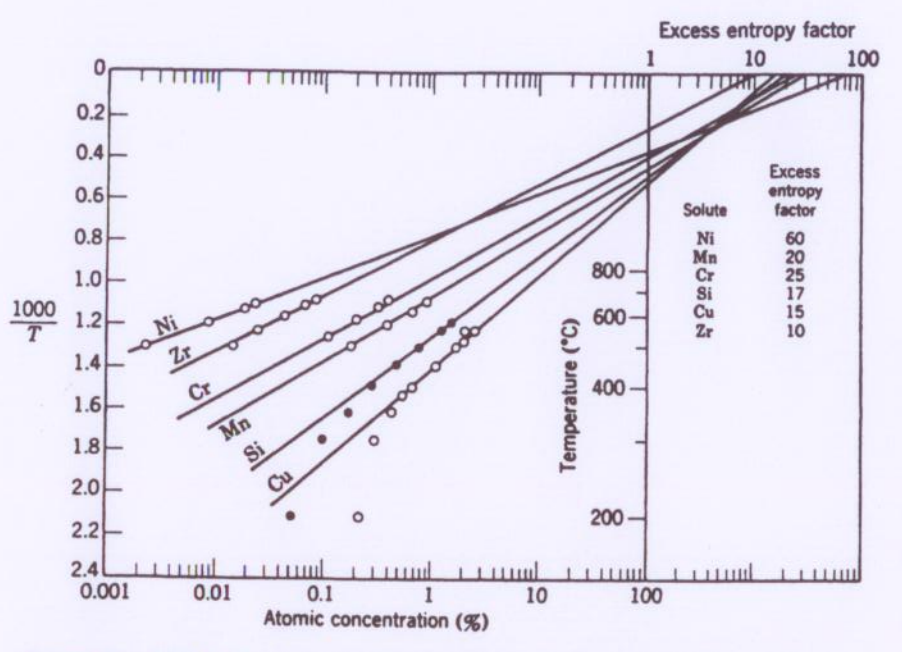


Figure 2.16. Solubility of solutes in aluminum plotted according to Eq. (2.31) to obtain ΔH_B and ΔS_B . From [18,19].

$$\Delta H_B = \Delta H_B^{\alpha\beta} + \Omega \tag{2.32}$$

and $\Delta H_B^{\alpha\beta}$ must be included in any calculation to extract Ω [12,14], as discussed further in the next section.

It is noted that, in general, the larger the value of ΔH_B , the higher is the value of ΔS_B . This can be understood, because a large value of ΔH_B is often associated with a large misfit of the solute in the crystal, which lowers the vibrational frequencies of neighboring atoms and results in a positive contribution to ΔS_B .

2.8. CALCULATION OF REGULAR SOLUTION PARAMETER AND ϵ_{AB} FROM PHASE DIAGRAMS

Once ΔH_B is determined from Eq. (2.31), it is possible to obtain the interaction parameter Ω from Eq. (2.25) by noting that, for a regular solution,

$$\Delta H_{\text{mix}} = \Omega (1 - X_B)^2 \tag{2.33a}$$

and, in the limit of a dilute solution, where $X_B \rightarrow 0$ (refer to Fig. 2.5),

$$\Delta H_{\text{mix}} = \Delta H_B = \Omega. \tag{2.33b}$$

Hence, we have a convenient way of obtaining Ω from the heat of solution ΔH_B . The value of ϵ_{AB} can then be obtained from Ω using Eqs. (2.19) and (2.22) with values for ϵ_{AA} and ϵ_{BB} estimated from an equation such as Eq. (1.4). As mentioned in the previous section, this procedure is valid when the α and β phases have the same crystal structure so that there is no change in standard state when dissolving 1 mole of β with the α structure into β to make a dilute solution.

Table 2.1 shows the heats of solution for single substitutional impurities in a variety of f.c.c. alloys [7] calculated using the embedded atom method (EAM) and compared with experimental values obtained from Hultgren et al. [20]. The energies are given in electron volts per atom. Similar calculations have been performed by Johnson [21]. The agreement between the calculated and experimental heats of solution is generally good to within about 0.1 eV, indicating the utility of performing sophisticated atomistic calculations in model systems. The values are consistent with the phase diagrams of the alloys [22, 23]. For example, the nickel-silver system is immiscible up to the melting point, which is consistent with the large positive heats of solution in Table 2.1. For the platinum-gold system, there is a miscibility gap over a large part of the composition range, which indicates a positive heat of solution as found in the calculations. The palladium-platinum system forms a continuous series of solid solutions at high temperatures, although there is evidence of a miscibility gap near 1050 K. This suggests that the heats of solution should be small but positive. The platinum-silver system forms a variety of ordered phases, which indicates that the platinum-silver interaction is attractive relative to the platinum-platinum and silver-silver interactions, as reflected in the negative heats of solution in Table 2.1.

Table 2.1. Heats of solution (in eV/atom) for various f.c.c. alloys calculated from the embedded atom method [7] and compared with experimental values obtained from the heats of mixing in Huitgren et al. [20] (from [7])

			F	lost		
	Cu	Ag	Au	Ni	Pd	Pt
Cu		0.18	-0.12	0.06	-0.33	-0.38
		0.25	-0.13	0.11	-0.39	-0.30
Ag	0.11		-0.11	0.42	-0.36	-0.18
	0.39		-0.16		-0.11	
Au	-0.18	-0.11		0.30	-0.15	0.07
	-0.19	-0.19		0.28	-0.20	
Ni	0.04	0.38	0.08		-0.15	-0.25
	0.03		0.22		-0.09	-0.33
Pd	-0.34	-0.24	-0.12	0.07		0.03
	-0.44	-0.29	-0.36	0.06		
Pt	-0.54	-0.07	0.09	-0.28	0.04	
	-0.53			-0.28		

To illustrate calculation of Ω and ϵ_{AB} , consider the silver-copper phase diagram in Figure 2.17. We can use one of several methods to find Ω and ϵ_{AB} . If we use the silver-rich side of the phase diagram, we can calculate ΔH_B from Eq. (2.31) and then extract Ω using Eq. (2.33). Table 2.2 provides all the data necessary to perform this calculation. A plot of $\ln X_B^{\rm sat}$ versus 1000/T yields a slope $\Delta H_B/k_B$ given by

$$\Delta H_B/k_B = -\frac{1.96 - 5.65}{(2.11 - 0.95) \times 10^{-3} \text{ K}^{-1} = 3181.0} \text{ K}.$$

Thus,

$$\Delta H_B = (3181.0 \text{ K})(1.38 \times 10^{-23} \text{ J/K})(1 \text{ eV}/1.602 \times 10^{-19} \text{ J}) = 0.27 \text{ eV/atom}.$$

Note that this value is in good agreement with the experimental value of 0.25 eV/atom given in Table 2.1. From Eq. (2.33), the value of $\Omega_{AgCu} = \Delta H_B = 0.27$ eV/atom (or 26,447 J/mol). Using Eq. (2.22),

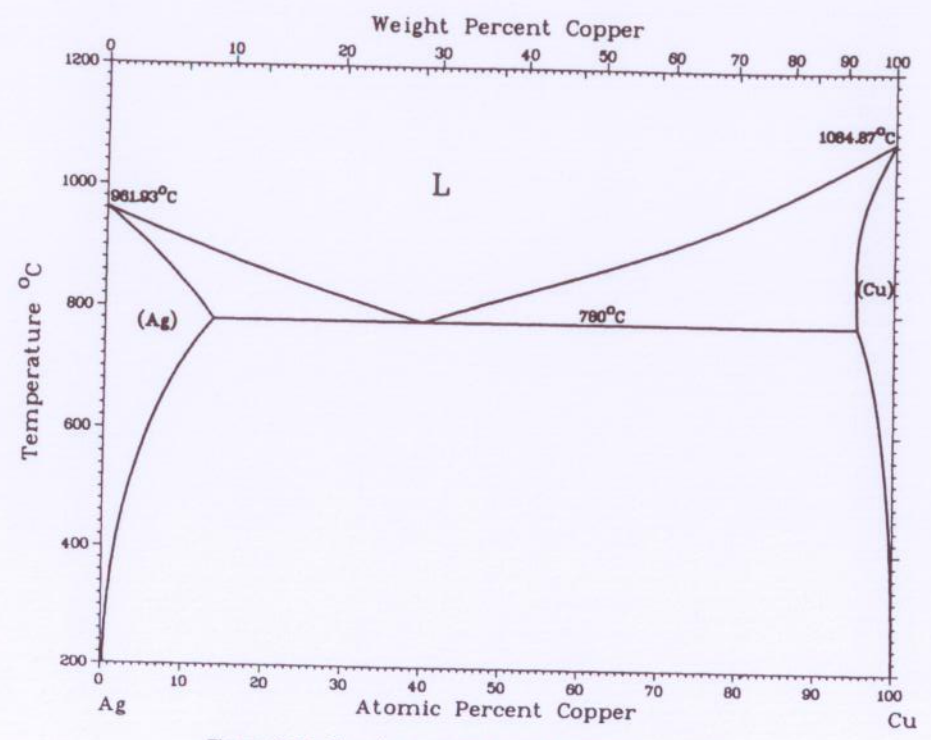


Figure 2.17. The silver-copper phase diagram. From [23].

Table 2.2. Solubility of copper in silver as a function of temperature obtained from the phase diagram in Fig. 2.17 and related parameters

Temp. [°C (K)]	Cu (at.%)	ln X sat◆	$1000/T (K^{-1})$
779 (1052)	14.1	-1.96	0.95
750 (1023)	11.9	-2.13	0.98
700 (973)	9.5	-2.35	1.03
600 (873)	5.5	-2.90	1.15
500 (773)	3.0	-3.51	1.29
400 (673)	1.2	-4.42	1.49
300 (573)	0.7	-4.96	1.75
200 (473)	0.35	-5.65	2.11

^{*}This is the natural logarithm of atomic fraction.

$$\epsilon_{AgCu} = \frac{\Omega_{AgCu}}{z} = \frac{0.27 \text{ eV/atom}}{12} = 0.023 \text{ eV/bond}.$$

Notice that $\epsilon_{AgCu} > 0$, consistent with phase separation and a eutectic phase diagram as in Figure 2.17. Now, if we use Eq. (2.19) and take the energies of the copper-copper and silver-silver bonds as the heats of sublimation given in Appendix B (or Table 1.1), we obtain

$$\epsilon_{AgCu} = \epsilon + \frac{1}{2}(\epsilon_{AgAg} + \epsilon_{CuCu}) = 0.023 + \frac{1}{2}(-0.49 + -0.58) = -0.51 \text{ eV/atom pair.}$$

This is the energy of the silver–copper bond. Alternatively, Ω_{AgCu} could have been determined by extrapolating the solvus lines on both sides of the silver–copper phase diagram up to the metastable miscibility gap. The value of T_c thus obtained (~ 1200°C) can then be used with Eq. (2.28) to obtain Ω_{AgCu} . The value for ε_{AgCu} would then be found from Ω_{AgCu} exactly as above. As a third possibility, one can use an average value for Ω_{AgCu} obtained from the solvus lines on both sides of the silver–copper phase diagram.

2.9. GENERALITY OF THE REGULAR SOLUTION MODEL

In closing this section on the regular solution model, it is important to note that, although we have developed the quasi-chemical model of a regular solution for metallic alloys, regular solution behavior has more general applicability and a parallel treatment exists for polymer solutions, for example. This treatment is often referred to as the Flory-Huggins theory [24], and it can account for the equilibrium properties of polymer solutions, particularly the large negative deviations from Raoult's law, phase separation, fractionation behavior, melting point depressions in crystalline polymers and swelling of networks. In the context of this book, the behavior of polymer interfaces is often modeled by combining the Flory-Huggins theory with the Cahn-Hilliard diffuse interface theory [25] (or square gradient interface

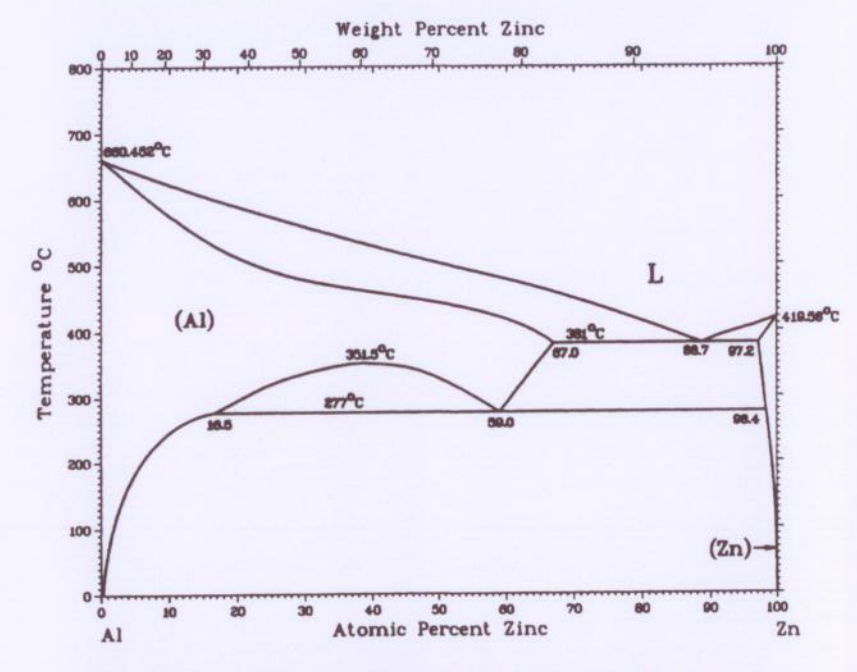
theory as it is often called in the polymer literature [26]), similar to what is often done in metallic alloys. We look at this theory in detail in Part IV.

The main difference between the Flory-Huggins theory for polymers and the quasi-chemical model we have just developed is that the Flory-Huggins theory takes into account the connectivity of polymer chain segments in the configurational entropy (Eq. 2.8) and also the effect of contact interactions between the solvent and the sides and ends of the polymer segments in the free energy of mixing (Eq. 2.7). This treatment results in an expression for the entropy of mixing, which is analogous to Eq. (2.9) and to a Flory-Huggins polymer-solvent interaction parameter (commonly labeled χ) which is analogous to Ω in Eq. (2.22). Hence, there is a useful parallel between these different materials which is relevant in the context of interfaces.

PROBLEMS

- 2.1. Using Eqs. (2.14) and (2.15), show that the chemical potentials of A and B can be obtained by extrapolating the tangent to the G-X curve to $X_A=0$ and $X_B=0$.
- 2.2. Derive Eq. (2.24) from Eqs. (2.15) and (2.23).
- 2.3. Gold (15 g) and silver (25 g) are mixed to form a single-phase ideal solid solution.
 - (a) How many moles of solution are there?
 - (b) What are the mole fractions of gold and silver?
 - (c) What is the molar entropy of mixing?
 - (d) What is the total entropy of mixing?
 - (e) What is the molar free-energy change at 500°C?
 - (f) What are the chemical potentials of gold and silver at 500°C, assuming the free energies of pure gold and silver are zero?
 - (g) How much will the free energy of the solution change at 500°C if one gold atom is added? Express your answer in eV/atom.
- 2.4. In a f.c.c. cubic lattice containing 40 at.% A and 60 at.% B in the form of a random solid solution, calculate the number of A-A, B-B and A-B pairs in a mole of solution.
- 2.5. Components A and B form a regular solution in the solid state for which $\Delta H_{\rm mix}$ is 20,000 $X_A X_B$ (J/mol). At a temperature of 1000 K, calculate the composition of α' and α'' in equilibrium and the composition of the inflection points.
- 2.6. Components A and B have melting temperatures of 1000 K and 900 K, respectively. Regular solutions form with ΔH_{mix} equal to $(20,000/T)X_AX_B$ and $(200,000/T)X_AX_B$ (J/mol) in the liquid and solid states, respectively.
 - (a) Will a minimum occur in the solidus and liquidus?
 - (b) If so, calculate the temperature of the minimum.

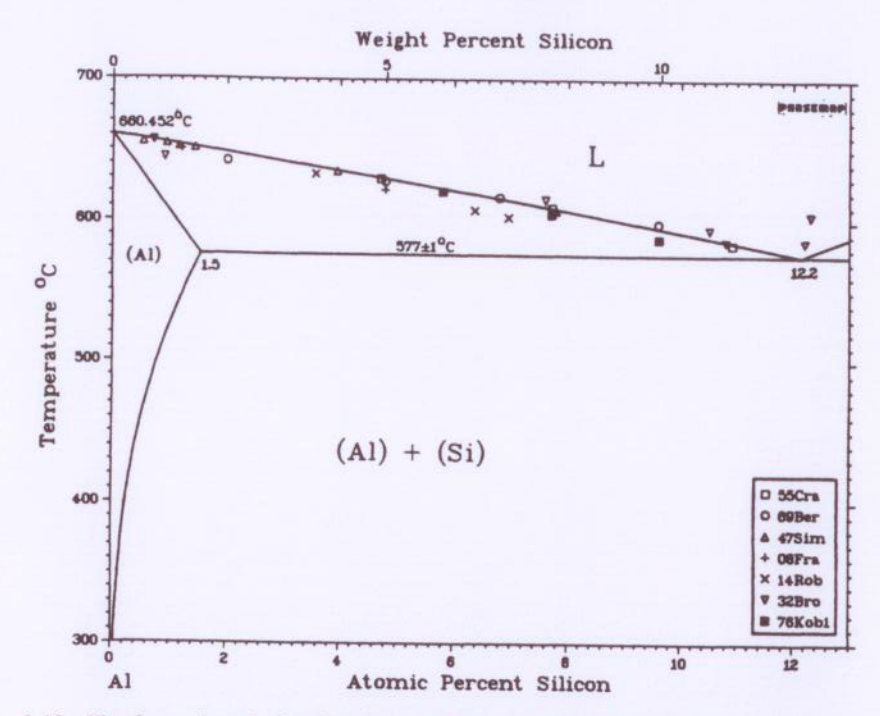
- 2.7. The solid solubility of silicon in aluminum is 1.25 at.% at 550°C and 0.46 at.% at 450°C. What solubility would you expect at 200°C? Check your answer by referring to the published phase diagram shown in Problem 2.9.
- 2.8. The aluminum-zinc phase diagram is shown below (from [23]).



- (a) Estimate €AIZn from the critical temperature in the phase diagram.
- (b) Estimate ϵ_{AlZn} from the solvus line in the phase diagram.
- (c) How do the results in (a) and (b) compare? Why?
- 2.9. The aluminum—silicon phase diagram is shown on page 40 (from [23]). Calculate €_{AlSi} from the solvus line in the phase diagram using Eq. (1.4) to estimate €_{AlAI} and €_{SiSi}. Explain any assumptions used in the calculations.
- 2.10. Based on the data for $\ln X_B^{\rm sat}$ versus 1/T shown in Figure 2.16, rank (do not calculate) the relative values of Ω for the solutes copper, manganese and nickel.
- 2.11. The f.c.c. gold—nickel phase diagram is shown on page 41 (from [23]). Estimate Ω_{AuNi} and ϵ_{AuNi} from T_{c} in the diagram. How does your value of Ω_{AuNi} compare with the heat of solutions given in Table 2.1? Explain any differences.
- 2.12. Using the regular solution model and the data in the table below, construct the phase diagram for the copper-nickel system and compare it with the accepted phase diagram (refer to [23]).

41

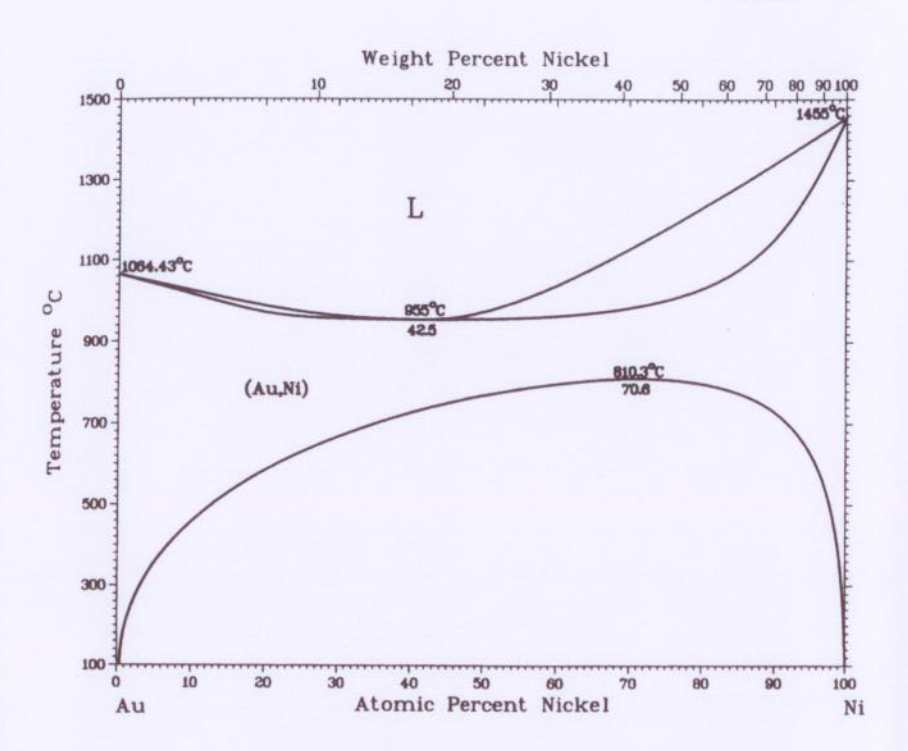
X_{Cu}	G (cal) $T = 973$ K
0.1	-415
0.2	-578
0.3	-654
0.4	-679
0.5	-667
0.6	-625
0.7	-559
0.8	-469
0.9	-334

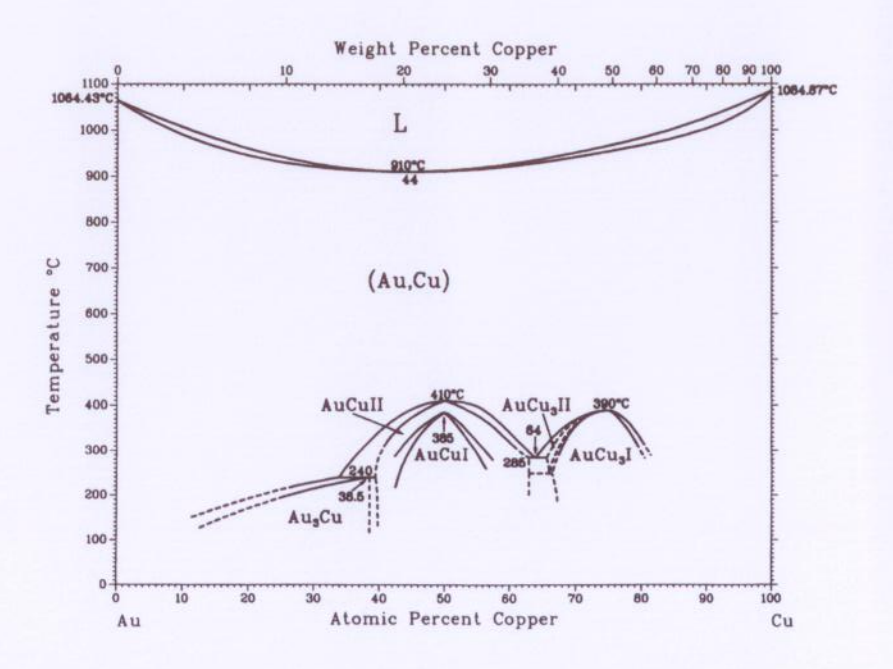


2.13. The f.c.c. phase in the aluminum-zinc system exhibits a miscibility gap (refer to Problem 2.8). Calculate the critical temperature and composition assuming that the molar Gibbs free energy is given by

$$G = X_A G_A + X_B G_B + RT(X_A \ln X_A + X_B \ln X_B)$$
$$+ X_A X_B (3,150X_A + 2,300X_B)[(1 - T/4000)] \text{ cal.}$$

2.14. The f.c.c. gold-copper phase diagram is shown on page 41 (from [23]). Calculate Ω_{AuCu} for the AuCu-I phase from T_{c} in the diagram. How does this value compare with Ω_{AuNi} in Problem 2.11? Explain any differences.





REFERENCES AND ADDITIONAL READING

REFERENCES

- K. N. Tu, J. W. Mayer and L. C. Feldman, Electronic Thin Film Science for Electrical Engineers and Materials Scientists, Macmillan, New York (1992), p. 22, 24, 66, 78.
- 2. R. J. Borg and G. J. Dienes, *The Physical Chemistry of Solids*, Academic Press, San Diego (1992), Chs. 3–8.
- 3. G. Burns, Solid State Physics, Academic Press, Orlando (1985), Ch. 6.
- C. Kittel, Introduction to Solid State Physics, 5th ed., John Wiley, New York (1976), p. 82.
- 5. M. S. Daw and M. I. Baskes, Phys. Rev. Lett., 50, 1285 (1983).
- 6. M. S. Daw and M. I. Baskes, Phys. Rev. B, 29, 6443 (1984).
- 7. S. M. Foiles, M. I. Baskes and M. S. Daw, Phys. Rev. B, 33, 7983 (1986).
- 8. A. D. McLean and R. S. McLean, At. Data Nucl. Data Tables, 26, 197 (1981).
- K. Binder, Ed., Monte Carlo Methods in Statistical Physics, 2nd ed., Springer, Berlin (1986).
- 10. S. M. Foiles, in *Equilibrium Structure and Properties of Surfaces and Interfaces*, A. Gonis and G. M. Stocks, Eds., Plenum Press, New York (1992), p. 89.
- 11. W. G. Hoover, Molecular Dynamics, Springer, Berlin (1986).
- D. A. Porter and K. E. Easterling, Phase Transformations in Metals and Alloys, 2nd ed., Chapman & Hall, London (1992), Ch. 1.
- R. A. Swalin, Thermodynamics of Solids, 2nd ed., John Wiley, New York (1972), p. 141, 172.
- R. T. DeHoff, Thermodynamics in Materials Science, McGraw-Hill, New York (1993), p. 191, 275.
- 15. R. A. Walker and J. B. Darby, Acta Metall., 18, 1261 (1970).
- 16. B. L. Averbach, P. A. Flinn and M. Cohen, Acta Metall., 2, 92 (1954).
- 17. W. L. Bragg and E. J. Williams, Proc. R. Soc. [Lond.], 145A, 699 (1934).

- J. E. Hatch, Ed., Aluminum: Properties and Physical Metallurgy, American Society for Metals, Metals Park, OH (1984), p. 25.
- C. Zener, in Thermodynamics in Physical Metallurgy, American Society for Metals, Cleveland, OH (1950).
- R. Hultgren, P. D. Desai, D. T. Hawkins, M. Gleiser and K. K. Kelley, Selected Values of the Thermodynamic Properties of Binary Alloys, American Society for Metals, Metals Park, OH (1973).
- 21. R. A. Johnson, Phys. Rev. B, 41, 9717 (1990).
- 22. M. Hansen, Constitution of Binary Alloys, McGraw-Hill, New York (1958).
- T. B. Massalski, H. Okamoto, P. R. Subramanian and L. Kacprzak, Eds., Binary Alloy Phase Diagrams, Vols. 1–3, ASM International, Metals Park, OH (1986).
- R. J. Young and P. A. Lovell, Introduction to Polymers, 2nd ed., Chapman and Hall, London (1992), p. 141.
- 25. J. W. Cahn and J. E. Hilliard, J. Chem. Phys., 28, 258 (1958).
- I. A. Sanchez, Ed., Physics of Polymer Surfaces and Interfaces, Butterworth-Heinemann, Boston (1992), p. 4.

ADDITIONAL READING

- A. Cottrell, Introduction to the Modern Theory of Metals, The Institute of Metals, London (1988), p. 60.
- C. H. P. Lupis, Chemical Thermodynamics of Materials, Elsevier, New York (1983), Chs. 6-9.
- D. A. Young, Phase Diagrams of the Elements, University of California Press, Berkeley (1991), Ch. 3.
- D. R. Gaskell, Introduction to Metallurgical Thermodynamics, McGraw-Hill, New York (1973).
- M. Hillert, in Lectures on the Theory of Phase Transformations, H. I. Aaronson, Ed., The Metallurgical Society of AIME, Warrendale, PA (1975), Ch. 1.
- J. Hafner, From Hamiltonians to Phase Diagrams, Springer, Berlin (1987).
- J. A. Alonso and N. H. March, Electrons in Metals and Alloys, Academic Press, London (1989).
- P. Haasen, Physical Metallurgy, 2nd ed., Cambridge University Press, Cambridge (1986).